Origins and consequences of asymmetric nano-FTIR interferograms

Here, we provide additional explanations to help understand some aspects of the manuscript and replicate the results of our calculations.

1. NEAR-FIELD SPECTRUM OF DIFFERENT SAMPLES

All the insertion scattering coefficients used in our study were calculated using the finite dipole model (FDM). [1] In all calculations the following FDM parameters were used: $L = 300$, $g = 0.7 \exp 0.06i$, $R = 25$, $A = 50$. The layered systems were modeled by using the Fresnel-reflection coefficient for the dominant near-field component with in-plane momentum $q = 2.5 \cdot 10^5$ cm^{-1} instead of the electrostatic reflection factor β as described in Ref. [2].

A. Model material

Fig. S1 (a) shows the model dielectric function for a theoretical material consisting of three different types of resonances in the middle infrared. Fig. S1 (b) presents the second harmonic near-field amplitude and phase signals. This amplitude and phase were used to calculate the interferograms displayed in the main text Fig. 4.

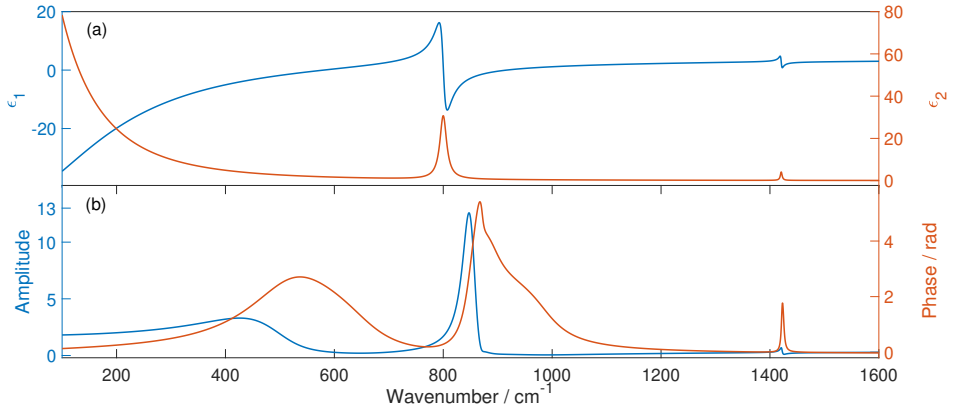

Fig. S1. (a) Model dielectric function ($\epsilon = \epsilon_1 + i\epsilon_2$) used to calculate near-field amplitude and phase spectra (b) with the FDM model.

B. Simple SiO_2/Si sample

Fig. S2 shows the near-field amplitude and phase spectrum of a 300 nm thick SiO_2/Si sample. The consists of the two broad phonon peaks of SiO_2 (≈800 and 1150 cm^{-1}).

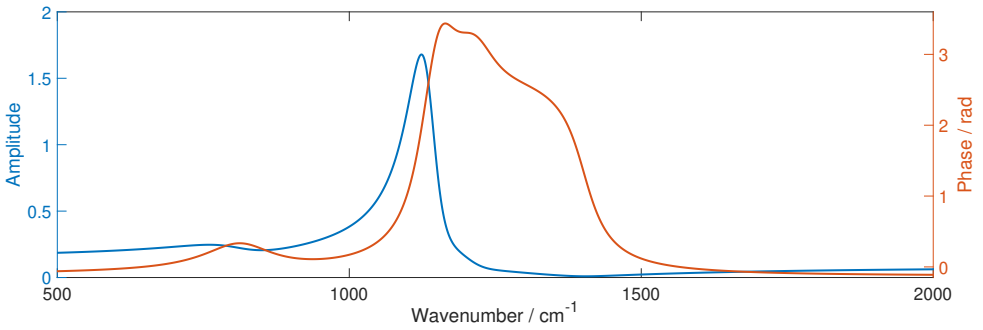

Fig. S2. Near-field amplitude and phase of the near-field scattering coefficient of SiO_2 300 nm-thick layer calculated using the FDM model.

C. C_{60} fullerene on top of SiO_2/Si

Fig. S3 shows the amplitude and phase spectrum of a 300 nm thick SiO_2/Si sample with 30 nm of C_{60} on top. The two broad phonon peaks of SiO_2 (800 and 1150 cm^{-1}) and two sharp vibrational lines of C_{60} (1184 and 1429 cm^{-1}) are clearly visible in the spectrum.

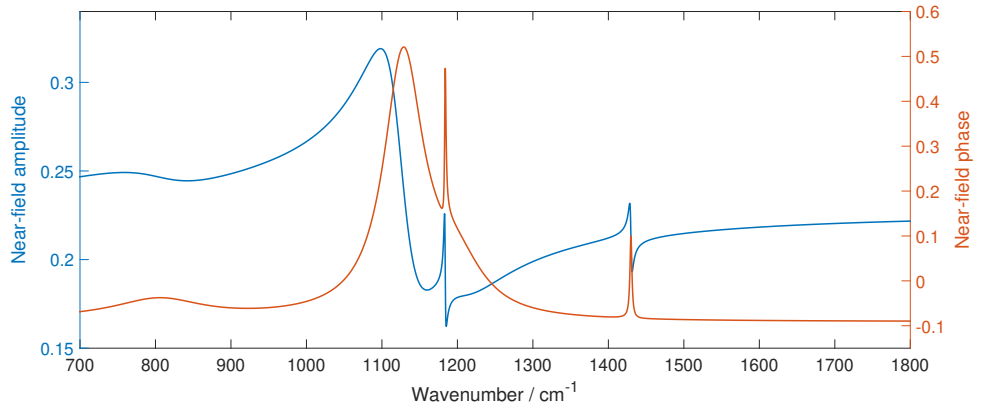

Fig. S3. Near-field amplitude and phase spectrum of the scattering coefficient of a $C_{60}/SiO_2/Si$ sample.

2. EFFECT OF ASYMMETRIC APODIZATION

In Section 4.2 of the manuscript, we mention that the asymmetric apodization in the extreme case can lead to the creation of a Kramers-Kronig pair phase spectrum. In such cases, the apodization

function is considered to be a Heaviside function ($\sigma(\delta)$) cutting the complete negative ZPD side of the interferogram (h(δ) - sample response). The resulting spectrum then can be written as:

$$F\{h(\delta)\cdot\sigma(\delta)\} = \frac{H(\omega) * F\{\sigma(\delta)\}}{\sqrt{2\pi}}. \tag{S1}$$

By evaluating the Fourier transform of the Heaviside function, expressing the convolution, and simplifying the equation, the Kramers-Kronig relations can be obtained. [3, 4]

$$H_{Re}(\omega) = \frac{2}{\pi}\int_0^\infty \frac{\omega' H_{Im}(\omega')}{\omega^2-\omega'^2}d\omega' \tag{S2}$$

$$H_{Im}(\omega) = \frac{-2}{\pi}\int_0^\infty \frac{\omega H_{Re}(\omega')}{\omega^2-\omega'^2}d\omega'. \tag{S3}$$

This means that when a symmetric interferogram (without phase spectrum) gets cut and becomes single-sided, the Fourier spectrum of the new interferogram will contain the Kramers-Kronig phase pair of the amplitude spectrum.

In case we change the symmetry of the original interferogram, we have to deal with an extra phase contribution that is coming from the effect described above. In Fig. S4 (a) and Fig. S4 (b), we show this by asymmetrically apodizing on an initially symmetric (without phase spectrum) interferogram. The figures show how the phase spectrum evolves with the symmetry change.

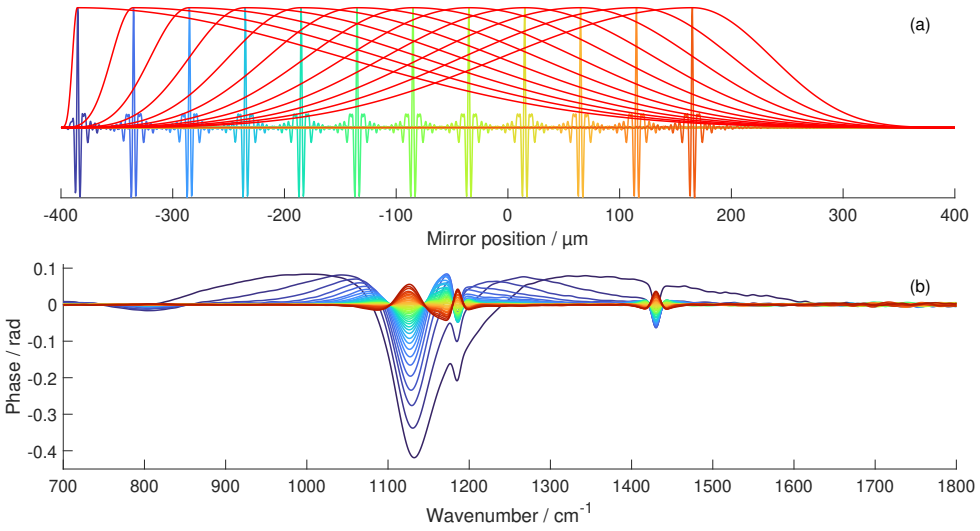

Fig. S4. (a) Symmetric, conventional reflection FTIR interferograms calculated for $C_{60}/SiO_2/Si$ sample with different ZPD positions and the corresponding apodization functions. (b) The phase spectra of the interferograms from (a). The introduction of more and more asymmetry results in the appearance of the Kramers-Kronig pair of the amplitude spectrum

3. COHERENT AND INCOHERENT SOURCE

In section 2.2 of the manuscript, we compared different light sources used in nano-FTIR spectroscopy. We identified that the main difference between them is temporal coherence. Broadband infrared DFG lasers provide coherent femtosecond pulses while synchrotrons and thermal emitters do not. However, the final interferogram is the same for both sources.

In the case of coherent pulses, the interferograms in the literature were interpreted in the framework of optical free induction decay (FID). During the scattering, the wavelength components of the back-scattered pulse suffer phase shifts and thus the back-scattered/emitted pulse becomes asymmetric exhibiting a long, decaying tail in the time domain. In the case of multiple sharp resonances, the tail also becomes a beating pattern. This is known as the FID signal. We show this effect with a very simple case in Fig. S5. We consider a laser source with a Gaussian spectrum (FWHM = 400 cm^{-1}) and a theoretical scatterer with one resonance as shown in Fig. S5 (a). For this situation, we show the electric field of the original (blue) and the scattered (red) pulse. The back-scattered pulse exhibits the decaying part for positive times which is usually identified as the FID tail.

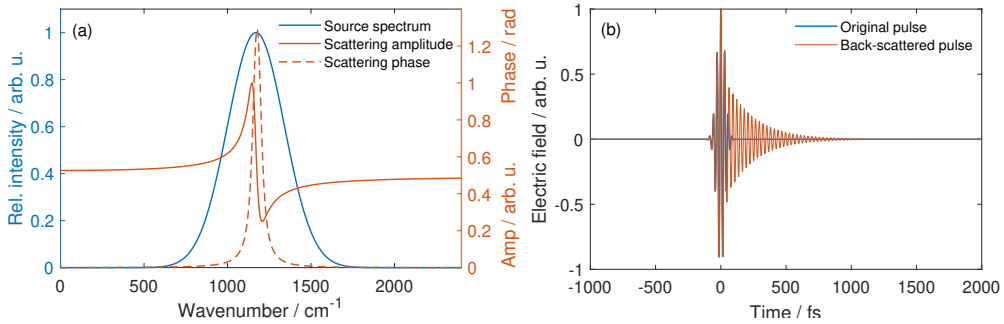

Fig. S5. (a) Spectrum of the light source and the amplitude and phase of an arbitrary sample with a single resonance. (b) the electric field of the original pulse and the distorted pulse caused by the scattering

In the case of an incoherent source, we do not have a well-defined pulse in time, since the wavelength components have a random phase relative to each other. Fig. S6 (a) and (b) show the electric field of a coherent pulse and an incoherent source with the same spectra plotted in Fig. S5 (a). We can compare the back-scattered field as well, which is shown in Fig. S6 (c) and (d), where (d) shows that with incoherent illumination there is no FID signal, there is no measurable decay in the fields in the time domain.

However, in the nano-FTIR setup, the detector signal as a function of the mirror position gives us the cross-correlation of the original and the back-scattered fields, i.e., the interferogram. In Fig. S6 (e) and (f), we present the calculated interferograms for the coherent and the incoherent fields shown before. The results very clearly show that the interferogram does not depend on the initial

phase relations of the incoming field but only depends on the phase shift between the original and the back-scattered field as we presented in the formulas of the main text. Based on this ambiguity of the interferogram, we think that it is a better approach to describe the nano-FTIR interferograms more generally based on the insertion loss than explaining them only by FID which is a special case but with the same origin.

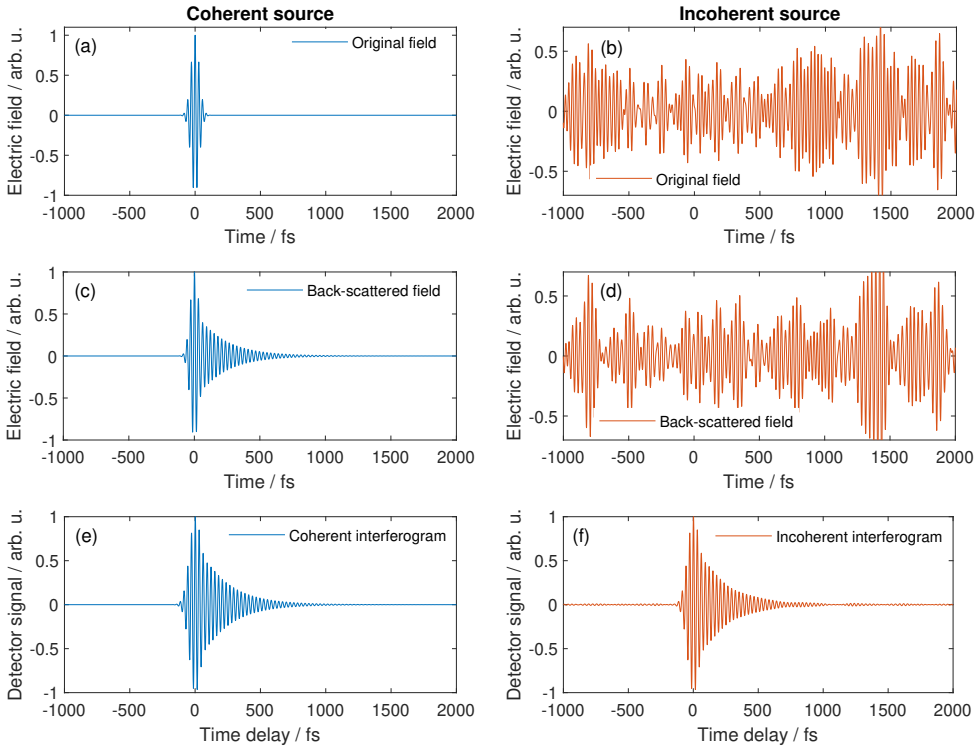

Fig. S6. Comparison of the electric fields of a coherent laser source (a), and an incoherent source (b) with the same spectrum. (c) and (d) are the back-scattered fields driven by the scattering coefficient plotted in Fig. S5. (e) and (f) are the interferograms calculated as the cross-correlation of the original and the scattered electric fields.

4. DERIVATION OF OPTIMAL ZPD SHIFT

At the end of the main text, we provide a simple formula to approximate the optimal ZPD position. We defined it in a way that the half maximum point of the normalized Gaussian (G(x)) envelope of the interferogram has to coincide with the 95% point of the apodization function which is a four-term Blackmann-Harris window (BH(x)), where x is the scanner position. The formulas for

our requirement are the following equations:

$$G(x) = 0.5 \quad = \quad e^{-x^2/\sigma^2} \tag{S4}$$

$$BH(x) = 0.95 \quad = \quad 0.35875 + 0.48829\cos\left(\frac{\pi}{L}x\right) + 0.14128\cos\left(\frac{2\pi}{L}x\right) \tag{S5}$$

$$+ \quad 0.01168\cos\left(\frac{3\pi}{L}x\right) \tag{S6}$$

Where L is the distance between the beginning of the scanner range and the maximum of the Blackmann-Harris function and $\sigma = \Delta_{IFG}/(2\sqrt{2\log(2)}))$ is the standard deviation of the Gaussian function. Both equations have to be solved for x and have to be equal,

$$x_{BH=0.95} \quad \approx \quad 0.09462L \tag{S7}$$

$$x_{G=0.5} \quad = \quad \sigma\sqrt{\log(4)} = \Delta_{IFG}\frac{1}{2}\sqrt{\frac{\log(4)}{2\log(2)}} = \Delta_{IFG}/2 \tag{S8}$$

$$x_{BH=0.95}(L) \quad = \quad x_{G=0.5}(\Delta_{IFG}) \tag{S9}$$

With the equivalence in Eq. S8, we end up with an expression for L as a function of the full width at half maximum (FWHM) of the Gaussian envelope of the interferogram. We note that $x_{BH=0.95}(L)$ has a very complex form and in Eq. S8 we approximate it with $0.0946L$, but in more general, we can use $x_{BH} = K \cdot L$, where K is a constant that varies depending on our criterion. At the end, L thus the ZPD position is:

$$L = \Delta_{IFG} \cdot \frac{1}{2K} = \frac{0.44}{\Delta_{LS}} \cdot \frac{1}{2K} \tag{S10}$$

where $K = 0.09462$. Since L is the distance from the beginning of the scanner range and the maximum of the apodization function that is centered on the ZPD point, this value directly gives us the desired position of the ZPD measured from the edge of the scanner range. We want to note that the value of K depends on how strict is our requirement. For example, if we loosen up our criterion and allow the shift until $x_{BH=0.80} = x_{G=0.5}$, it would become $K = 0.1967$ but this would allow shifting the ZPD position far closer to the edge of the scanner range and thus would result in serious phase spectrum distortion. The criterion and the corresponding K value were chosen to fit the optimum ZPD shift values from the actual spectrum calculations, shown in Fig. 15 of the main text. Fig. S7 shows an apodization function, a Gaussian interferogram envelope, and the corresponding interferogram that satisfy our criteria described above. The example calculation was done for a light spectrum with $\Delta_{LS} = 200\,cm^{-1}$. The vertical line coincides with $x_{BH=0.95}$ and $x_{G=0.5}$ as shown by the horizontal dashed lines.

REFERENCES

1. A. Cvitkovic, N. Ocelic, and R. Hillenbrand, "Analytical model for quantitative prediction of material contrasts in scattering-type near-field optical microscopy," Opt. Express **15**, 8550–8565 (2007).
2. B. Hauer, "Nano-optical mapping of permittivity contrasts and electronic properties at the surface and beneath," Ph.D. thesis, RWTH Aachen University (2015).

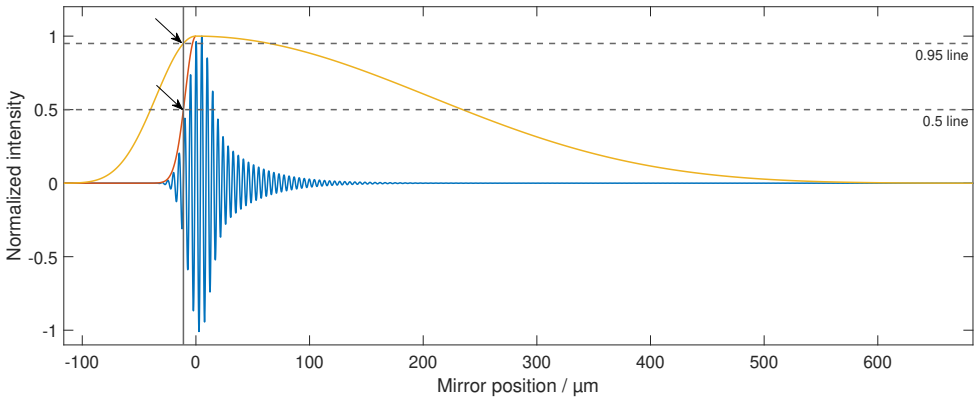

Fig. S7. Interfrogram and the corresponding apodization function that satisfies our ZPD placement criterion defined by Eq. S10., (yellow) Blackman–Harris apodization function, (red) interferogram envelope, (blue) interferogram.

3. "A simple derivation of the Kramers-Kronig relations from the perspective of system theory," https://www.iam.kit.edu/et/plainhtml/Download/Derivation_Kramers-Kronig.pdf. Accessed: 2024-01-15.
4. D. K. M. Schönleber and E. Ivers-Tiffée, "A method for improving the robustness of linear kramers-kronig validity tests," Electrochimica Acta pp. 20–27 (2014).